Chapter 1

SOLAR RADIATION ESTIMATION USING A NUMERICAL MODEL

F. Díaz, J.M. Escobar, E. Rodríguez, R. Montenegro, G. Montero[*]

University Institute for Intelligent Systems and Numerical Applications in Engineering
University of Las Palmas de Gran Canaria

Abstract

A solar radiation numerical model is presented. It is intended to be useful for different purposes like the evaluation of the suitability of possible locations for solar power stations. This model allows the user to evaluate the radiation values in any location easily, and estimate the solar power generation taking into account not only the radiation level, but also the terrain surface conditions considering the cast shadows. The solar radiation model is implemented taking into account the terrain surface using 2-D adaptive meshes of triangles, which are constructed using a refinement/derefinement procedure in accordance with the variations of terrain surface and albedo. The selected methodology defines the terrain characteristics with a minimum number of points so that computational cost is reduced for a given accuracy. The model can be used to find the optimal location for obtaining the maximum power generation. For this purpose, the effect of shadows is considered in each time step. Solar radiation is first computed for clear sky conditions, considering the different components of radiation: beam, diffuse and reflected radiation. The real sky radiation is computed daily starting from

[*]E-mail address: gustavo@dma.ulpgc.es

the results of clear sky radiation, in terms of the clear sky index. Maps for clear sky index are obtained from a spatial interpolation of observational data which are available for each day at several points of the zone under consideration. Finally, the solar radiation maps of a month are calculated from the daily results. The model can be also applied in solar radiation forecasting. To do so, a forecasting meteorological model is required. The estimation of daily solar radiation provided by such model is used to adjust the clear sky results and obtain the real sky radiation. Some numerical experiments related to the generation of solar radiation maps in Gran Canaria Island (Canary Islands - Spain) are presented. **Keywords:** solar radiation, shadows, adaptive meshes, solar power.

1   Introduction

Solar radiation affects all physical, chemical and biological processes on earth. Therefore, the knowledge about it is relevant in meteorology, forestry, agronomy, geography, medicine and, of course, in power generation. In this topic, the importance of the renewable energies in our world is greater each day. Factors like the oil shortage or the climate change related to the global warming, have caused a high increase in the development of the different renewable energy technologies. Between them, solar power has become very important due to the support of the authorities and the research in this field. Part of this research is the development of some solar radiation numerical models. These models need to take into account the interaction of the radiation with the terrestrial atmosphere and surface, this is [1, 2]:

1. The geometry of the Earth (declination, latitude, solar hour angle)
2. The terrain characteristics (elevation, albedo, surface inclination and orientation, shadows)
3. The atmospheric attenuation (scattering, absorption) caused by gases, particles and clouds

Considering the three factors of atmospheric attenuation in a model, it will produce real sky radiation values. If we omit the cloud attenuation, clear sky (cloudless) radiation values will be obtained.

Two main groups of spatial models for solar radiation can be found. On one hand there are those models based on the study of data obtained from satellite observations [3], and, on the other, those based on astrophysical, atmosphere physical and geometrical considerations [1, 2].

Starting from the works of Šúri and Hofierka [1, 2] regarding a GIS-based solar radiation model, the calculation of solar radiation on the terrain [4, 5] is studied. Determining the influence of the orography and the terrain characteristics in the radiation is very important to reach accurate results. In fact, the factors related to the terrain such as the elevation, the albedo, the surface inclination or the cast shadows, are essential to have a precise idea of how the radiation comes into contact with the surface. The shadowing effect over a surface has been studied by Niewienda et al. [6] who propose calculating the GSC (geometrical shading coefficient) this is, the proportion of shaded area of an arbitrarily oriented surface surrounded by shading elements, as a function of time and location. Zakšek et al. [7] propose a solar radiation model based on defining the incidence angle by computing

normal-to-the-surface tangent plane and direction of the Sun. Since they use a regular grid in their computations, the computational cost of this approach is higher than others using an adaptive discretization. Other methods [8, 9] do not consider a solid surface and, thus, need a high density of sample points in order to obtain accurate results.

In this chapter, a solution for the estimation of the solar radiation on the terrain with a low computational cost is presented. We will use an adaptive mesh of triangles [4, 5] to represent the terrain and its actual orography as a solid surface that really casts shadows and so it is not as sensitive as the former to the density of sample points. Mesh refinement/derefinement techniques which have been widely used in other scientific problems [10, 11, 12, 13] have been applied. For example, the implementation of the 4-T Rivara's refinement algorithm [14] and a derefinement algorithm [15], developed by Ferragut et al. [11] are good choices to reach our terrain mesh. For solar collectors, the application of our model is straightforward. It can determinate the terrain-induced shading on collectors.

To summarize, this adaptive model allows the refinement of the results of a GIS-based model, which would have a high computational cost, in accurate local area simulations. In addition, this model may be connected to a GIS tool as a local solver.

2   Modelling of geographical features

As said above, the terrain characteristics, including albedo, shape or inclination, are very important for the knowledge about the hourly and daily radiation values. Related to this, we will have to take into account two main issues: the construction of an accurate *terrain mesh*, and the *detection of shadows*.

2.1   Terrain surface mesh

The terrain surface mesh must be constructed taking into account both, orography and albedo. As Montero et al. [4] described, an adaptive procedure of mesh refinement/derefinement has been carried out using two different derefinement parameters. This is not the only applicable method since a Delaunay triangulation or other more complex methods can be applied to get specific features like ridges or valley bottoms. However, nested meshes are used because we need to transfer information along an evolution process (shadow and radiation) from mesh to mesh.

The first step to make the mesh generation is the determination of nodes allocated on the terrain surface. Their distribution must be adapted to the orographic and albedo characteristics in order to minimize the number of required nodes for a given accuracy. Starting from a regular triangulation τ_1 of the rectangular region under study, a sequence of nested meshes $\Gamma = \{\tau_1 < \tau_2 < \ldots < \tau_m\}$ will be builded. The triangulation is such that the level τ_j is obtained by a global refinement of the previous level τ_{j-1} with the 4-T Rivara's algorithm [14], this is, each triangle of level τ_{j-1} is divided into four subtriangles inserting a new node in the middle of the edges and linking the node in the longer edge with the opposite vertex and with the remaining two new nodes. The number of levels m of the sequence is determined by the degree of discretization of the terrain, so we can ensure that this regular mesh is able to capture all the orographic and albedo information by an interpolation of the heights and albedo in the nodes of the mesh.

Once this is done, we have to define a new sequence $\Gamma' = \{\tau_1 < \tau'_2 < \ldots < \tau'_{m'}\}, m' \leq m$, by applying the derefinement algorithm [11, 15]. By means of two derefinement parameters, ε_h and ε_a, we can determine the accuracy of the approximation to terrain surface and albedo. The absolute difference between the height obtained in any point of the mesh $\tau'_{m'}$ and the corresponding exact height will be lower than ε_h.

2.2   Detection of shadows

The accurate estimation of the solar radiation on a terrain surface needs to take into account the cast shadows. This problem is, after all, a geometrical one: a triangle will be shadowed when, looking at the mesh from the sun, we can find another triangle that totally or partially covers the former.

One way to face this issue is constructing a reference system x', y' and z', with z' in the direction of the beam radiation (see Figure 1). After this, the mesh needs to be projected on the plane $x'y'$.
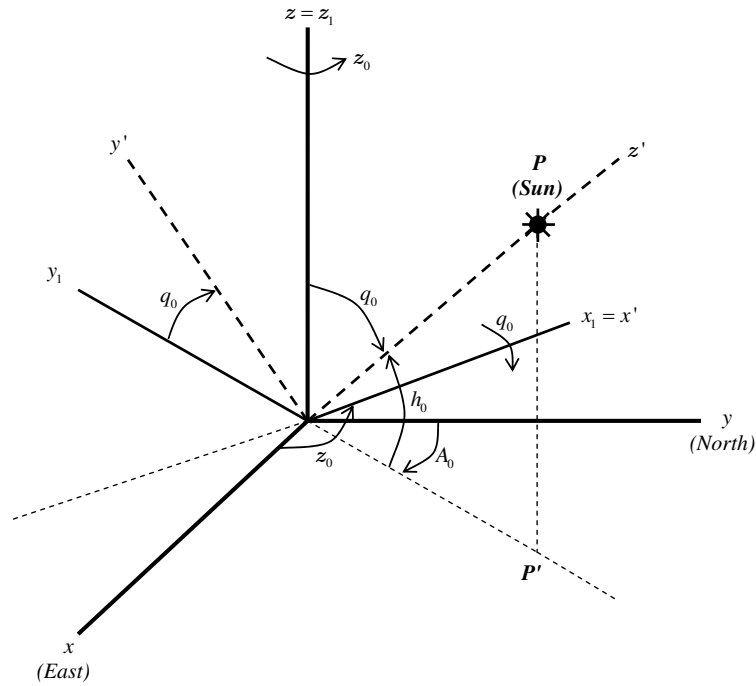
Figure 1. Reference systems and Euler angles

The sun position with respect to a horizontal surface is given by two coordinates, the solar altitude h_0 and the solar azimuth A_0 (see Figure 1), which are calculated as,

$$\sin h_0 \quad = \quad \cos\varphi\cos\delta\cos T + \sin\varphi\sin\delta \tag{1}$$

$$\cos A_0' \quad = \quad \frac{\sin\varphi\cos\delta\cos T - \cos\varphi\sin\delta}{\sin h_0} \tag{2}$$

$$\text{if} \qquad \sin T > 0, \qquad A_0 = -A_0'$$

$$\text{if} \qquad \sin T \le 0, \qquad A_0 = A_0'$$

T is the hour angle (rad) obtained from equation (5), φ the latitude in radians and δ the sun declination in radians obtained according to Gruter [16],

$$\sin\delta = 0.3978\sin\left[j' - 1.4 + 0.0355\sin(j' - 0.0489)\right] \tag{3}$$

with j' being the day angle represented in radians as follows,

$$j' = \frac{2\pi j}{365.25} \tag{4}$$

Here j is the day number which varies from 1 on January 1st to 365 on December 31st. The hour angle T (rad) is calculated from the local solar time t expressed in decimal hours on the 24 hour clock as

$$T = \frac{\pi}{12}(t - 12) \tag{5}$$

As said above, we need to make a coordinate transformation to get z' in the direction of the beam radiation. Thus, we need to know a vector that defines the solar beam direction for any time and position. In the literature we can find many ways to reach this. Blanco-Muriel et al. proposed the so called PSA algorithm [17], developed at the *Plataforma Solar de Almería*. Niewienda and Heidt stated a simple vector to define this direction [6].

$$v_{sol} = \begin{pmatrix} \cos h_0 \sin A_0 \\ \cos h_0 \cos A_0 \\ \sin h_0 \end{pmatrix}$$

For each triangle two angles are computed, the azimuth A_N (angle between the horizontal normal projection and East), and γ_N (angle between the normal to the triangle and the horizontal plane). The solar incidence angle δ_{exp} is then computed for each triangle [18, 19]. Please note that these new references will only be used for the determination of this angle.

$$\sin\delta_{exp} \quad = \quad \cos\varphi'\cos\delta\cos(T - \lambda') + \sin\varphi'\sin\delta \tag{6}$$

where

$$\sin\varphi' = -\cos\varphi\sin\gamma_N\cos A_N + \sin\varphi\cos\gamma_N \tag{7}$$

$$\tan\lambda' = -\frac{\sin\gamma_N\sin A_N}{\sin\varphi\sin\gamma_N\cos A_N + \cos\varphi\cos\gamma_N} \tag{8}$$

Once this is done, the intersection between triangles is checked. This analysis involves a high computational cost. To diminish this cost we have considered four warning points for each triangle as can be seen in Figure 2, left. This is not the only possibility since we can, if
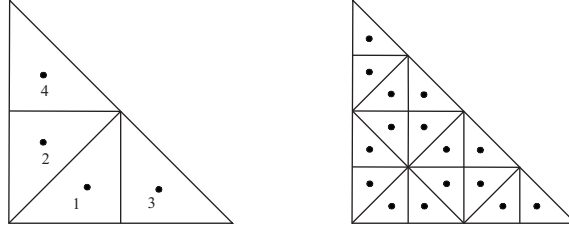
Figure 2. Warning points for shading analysis

needed, add more precision to the shade detection simply increasing the number of warning points as can be seen in Figure 2 right, where now we have sixteen warning points instead of the former four points.

We assign a different level of lighting or shade to each triangle of the mesh depending on the number of warning points that lie inside other triangles. Specifically, a triangle Δ will have an associated lighting factor which, for the case of four warning points, will be

$$L_f = \frac{4 - i}{4} \tag{9}$$

with $i = 0, 1, 2, 3, 4$ being the number of warning points inside other triangles that are in front of Δ. Clearly, L_f is a quantity between 0 and 1. This factor is used below in the estimation of beam and diffuse irradiances.

3   Solar radiation modelling

Once the terrrain is discretized by means of adaptive meshes, it is time to calculate the radiation values on every triangle. This will be done using a *solar radiation model* based on the work of Šúri and Hofierka [1, 2]. The obtained values are computed for each time step, taking into account the shadows over each triangle of the surface [4], by using the method described above.

The results that we would have right now, are the clear sky radiation values, this is, the solar radiation values considering clear sky conditions. However, since the weather characteristics are a tremendous influence on the true radiation values that reach the surface, it is essential to take them into account. This way we will obtain the real sky values. Due to its random nature, the approach to this matter needs the knowledge of some of the actual existing meteorological variables in a place. The simplest and most accurate way to face this issue is using observational radiation data available from different measurement stations. We can now analyze the real sky radiation values for a chosen day or month for the whole spatial desired zone, or we can decide to make a previous statiscal analysis of the observational data to get more accurate results about what real sky radiation we can expect in a place in a certain date and time of the year. The statiscal analysis of the available data will give a *Typical Meteorological Year* (TMY) [20, 21] which will be the starting point to convert the clear sky into real sky.

Finally, the calculations flow would be:

1. Solar radiation calculation for all the mesh, assuming clear sky conditions

2. TMY calculation for all the involved mesurement stations
3. Correction of the solar radiation values using the measured values to reach the real sky conditions

Steps one and three are repeated for each time step and finally the total solar radiation value is obtained integrating all the instantaneous values.

3.1 Solar radiation equations for clear sky

The global solar irradiance comprises three different components: *beam*, *diffuse* and *reflected* irradiances. The first one, though partially attenuated by the atmosphere, is not reflected or scattered and reaches the surface directly. The second one is the scattered irradiance that reaches the terrain surface and that goes in all directions and produces no shadows of the inserted opaque objects. The third one is the irradiance which is reflected from the surface onto an inclined receiver and depends on the ground albedo.

The relative importance of these three kind of irradiances depends upon the sky conditions. In sunny days, the diffuse radiation would be no more than the 15% of the global radiation, while on overcast days its importance will be much greater. The reflected or albedo irradiance is the one with the lowest contribution to the global.

3.1.1 Beam radiation

According to J.K. Page [22], we will take the solar constant outside the atmosphere at the mean solar distance, I_0, as 1367 (W/m^2). Due to the earth's orbit eccentricity, a correction factor ε is needed for the calculation of the extraterrestrial irradiance G_0.

$$G_0 = I_0 \varepsilon \tag{10}$$

where $\varepsilon = 1 + 0.03344 \cos(j' - 0.048869)$, with j' being the day angle; see equation (4). The beam irradiance, normal to the solar beam, G_{b0} (W/m^2) is attenuated by the cloudless atmosphere, and calculated as follows:

$$G_{b0c} = G_0 \, exp\{-0.8662 T_{LK} m \delta_R(m)\} \tag{11}$$

The term $0.8662 T_{LK}$ is the dimensionless Linke atmospheric turbidity factor corrected by F. Kasten [23]. Subindex c shows that we are calculating clear sky irradiances. The parameter m in (11) is the relative optical air mass calculated using the formula [24],

$$m = \frac{p/p_0}{\sin h_0^{ref} + 0.50572(h_0^{ref} + 6.07995)^{-1.6364}} \tag{12}$$

where h_0^{ref} is the solar altitude in degrees corrected by the atmospheric refraction component Δh_0^{ref}, and p/p_0 is a correction for a given elevation z.

Taking into account what written above, the beam irradiance on a horizontal surface for clear sky conditions $G_{bc}(0)$ becomes,

$$G_{bc}(0) = G_{b0c} L_f \, \sin h_0 \tag{13}$$

where h_0 is the solar altitude angle and L_f, the lighting factor that corrects the beam irradiance as the surface is sunlit or shadowed. Then the beam irradiance on an inclined surface for clear sky conditions $G_{bc}(\beta)$ is obtained as,

$$G_{bc}(\beta) = G_{b0c}L_f \sin\delta_{exp} \tag{14}$$

where β is the angle between the inclined surface and the horizontal, and δ_{exp} is the solar incidence angle measured between the sun beam direction and its projection on an inclined surface. Note that, for horizontal surfaces, δ_{exp} coincides with h_0.

3.1.2 Diffuse radiation

The estimation of the diffuse component in horizontal surfaces $G_{dc}(0)(\text{W/m}^2)$ is carried out using the equation,

$$G_{dc}(0) = G_0 T_n(T_{LK})F_d(h_0) \tag{15}$$

As can be seen, $G_{dc}(0)$ is a function of the diffuse transmission T_n which, at the same time, depends on the Linke turbidity factor T_{LK}. Also, we have the function F_d which depends on the solar altitude h_0 [25].
The transmission function $T_n(T_{LK})$ will be,

$$T_n(T_{LK}) = -0.015843 + 0.030543T_{LK} + 0.0003797T_{LK}^2 \tag{16}$$

And, $F_d(h_0)$,

$$F_d(h_0) = A_1 + A_2 \sin h_0 + A_3 \sin^2 h_0 \tag{17}$$

where the values of A_1, A_2 and A_3 are,

$$
\begin{aligned}
A_1' &= 0.26463 - 0.061581T_{LK} + 0.0031408T_{LK}^2 \\
A_1 &= \frac{0.0022}{T_n(T_{LK})} \qquad \text{if } A_1'T_n(T_{LK}) < 0.0022 \\
A_1 &= A_1' \qquad\qquad \text{if } A_1'T_n(T_{LK}) \geq 0.0022 \\
A_2 &= 2.04020 + 0.018945T_{LK} - 0.011161T_{LK}^2 \\
A_3 &= -1.3025 + 0.039231T_{LK} + 0.0085079T_{LK}^2
\end{aligned}
\tag{18}
$$

To obtain the clear sky diffuse irradiance on a inclined surface with an angle γ_N, $G_{dc}(\gamma_N)(\text{W/m}^2)$,both, sunlit and shadowed surfaces (see section 2.2), have to be considered following the equations proposed in [26]. For sunlit surfaces ($L_f = 1$) the equations are,
If $h_0 \geq 0.1$ radians

$$G_{dc}(\gamma_N) = G_{dc}(0)\left(F(\gamma_N)(1-K_b) + K_b\frac{\sin\delta_{exp}}{\sin h_0}\right) \tag{19}$$

If $h_0 < 0.1$ radians

$$G_{dc}(\gamma_N) = G_{dc}(0)\left[F(\gamma_N)(1-K_b) + (K_b\sin\gamma_N\cos A_{LN})/(0.1-0.008h_0)\right] \tag{20}$$

where $A_{LN}^* = A_0 - A_N$

if $\quad -\pi \leq A_{LN}^* \leq \pi \quad$ then $\quad A_{LN} = A_{LN}^*$
if $\quad A_{LN}^* > \pi \quad$ then $\quad A_{LN} = A_{LN}^* - 2\pi$
if $\quad A_{LN}^* < -\pi \quad$ then $\quad A_{LN} = A_{LN}^* + 2\pi$

For shadowed surfaces ($L_f < 1$).

$$G_{dc}(\gamma_N) = G_{dc}(0)F(\gamma_N) \tag{21}$$

where $F(\gamma_N)$ is a function defined for the diffuse sky irradiance that may be computed as,

$$F(\gamma_N) = r_i(\gamma_N) + N\left(\sin\gamma_N - \gamma_N\cos\gamma_N - \pi\sin^2\frac{\gamma_N}{2}\right) \tag{22}$$

being $r_i(\gamma_N)$ a fraction of the sky dome viewed by an inclined surface,

$$r_i(\gamma_N) = (1 + \cos\gamma_N)/2 \tag{23}$$

The value of N for shadowed surfaces is 0.25227 while, for sunlit surfaces under clear sky, it is defined as,

$$N = 0.00263 - 0.712K_b - 0.6883K_b^2 \tag{24}$$

K_b is a proportion between beam irradiance and extraterrestrial solar irradiance on a horizontal surface,

$$K_b = G_{bc}(0)/G_0(0) \tag{25}$$

where

$$G_0(0) = G_0\sin h_0 \tag{26}$$

3.1.3 Reflected radiation

The last component to take into account is the ground reflected irradiance under clear sky ($G_r(\gamma_N)$). According to Muneer [27], this will be proportional to the global horizontal irradiance $G_c(0)$, to the mean ground albedo ρ_g and a fraction of the ground viewed by an inclined surface $r_g(\gamma_N)$.

$$G_r(\gamma_N) = \rho_g G_c(0) r_g(\gamma_N) \tag{27}$$

where

$$r_g(\gamma_N) = (1 - \cos\gamma_N)/2 \tag{28}$$
$$G_c(0) = G_{bc}(0) + G_{dc}(0) \tag{29}$$

3.2   Solar radiation under real sky

Once we have the clear sky radiation values, a correction to obtain the real sky values is necessary. This correction is needed due to the presence of clouds. The values of global radiation on a horizontal surface for real sky conditions $G(0)$ are calculated as a correction of those of clear sky $G_c(0)$ with the clear sky index k_c,

$$G(0) = G_c(0)k_c \qquad (30)$$

To calculate the clear sky index map on a zone, some measures of global radiation $G_s(0)$ (where subindex s means *station*) are needed. Therefore, it is mandatory to have some measurement stations with available data on the zone under consideration. In this case, the value of the clear sky index at each of those points may be computed as,

$$k_c = G_s(0)/G_c(0) \qquad (31)$$

At this point we have clear sky index (k_c) values only for the measurement stations. The next step will be the interpolation of the index for the whole zone. A simple formula that has also been used in other environmental problems defined on complex orography [28] is applied,

$$k_c = \varepsilon \frac{\sum_{n=1}^{N} \frac{k_{cn}}{d_n^2}}{\sum_{n=1}^{N} \frac{1}{d_n^2}} + (1-\varepsilon) \frac{\sum_{n=1}^{N} \frac{k_{cn}}{|\Delta h_n|}}{\sum_{n=1}^{N} \frac{1}{|\Delta h_n|}} \qquad (32)$$

where k_c corresponds to the clear sky index at each point of the mesh, k_{cn} is the clear sky index obtained at the measurement stations, N is the number of stations used in the interpolation, d_n is the horizontal distance and $|\Delta h_n|$ is the difference in height between station n and the studied point, respectively, and ε is a parameter between 0 and 1. In problems with regular orography or in two-dimensional analysis, we choose high values of ε. However, for complex terrains, lower values of ε are a better choice. Thus, since it is very common to have regions with both regular and irregular zones, an intermediate value of ε is more suitable. We have to include the case where the studied point coincides with a measurement station. In such cases, equation (32) is not continuous. The continuity is ensured if we assume the measured value at those points. To calculate the value of $G_b(0)$ and $G_d(0)$ under real sky, a similar procedure may be applied from experimental measures.

3.3   Typical meteorological year

To estimate the real sky radiation, we will use the actual radiation values obtained from several measurement stations (see 3.2). However, those data belong to a given moment and, using values from a single year would take us to a non reliable result since the used data are fruit of the weather conditions in that particular day of that year. To avoid this problem we need an accurate *typical meteorological year* (TMY). A revision of different methods to obtain a TMY can be seen in the work of Argiriou et al. [29].

   The method applied in this Chapter is described in [21], but a brief explanation can be seen in section 3.3.1 and in 3.3.2.

3.3.1   Time series analysis

As we can see in the literature, autoregressive moving average (ARMA) models are widely applied to time series [30]. A series can be adjusted by means of an additive way,

$$Y_t = \sum_i [\alpha_i cos(\omega it) + \beta_i sin(\omega it)] + \varepsilon_t \tag{33}$$

where ω is a constant and the deterministic part of the Y_t variability is a trigonometric series, and the random component, ε fits an ARMA model,

$$\varepsilon_t = \phi_1 \varepsilon_{t-1} + \ldots + \phi_p \varepsilon_{t-p} + a_t + \theta_1 a_{t-1} + \ldots + \theta_q a_{t-q} \tag{34}$$

The model orders are p and q, and its variability depends upon their inmediately previous values and a random series, a_t which satisfies the following:

$$E(a_t) = 0 \quad V(a_t) = \sigma_a^2 \quad Cov(a_t, a_{t-k}) = 0 \quad \forall t, k$$

To soften irregularities, moving averages are recommended. These ones can be adjusted by the least-squared method. Due to the cyclical character of our series, a Fourier analysis is a good choice. Having this in mind, Equation (33) becomes:

$$Y_t = \alpha_0 + \sum_{i=1}^{r} \left[\alpha_i cos \left(\frac{2\pi it}{T} \right) + \beta_i sin \left(\frac{2\pi it}{T} \right) \right] + \varepsilon_t \quad t = 1 \ldots n \tag{35}$$

being T the cycle period. The moving average method allows to minimize the time series noise, transforming Y_t series in another one by means of the following transformation,

$$MY_t = \sum_{j=-m}^{m} \omega_j Y_{t+j} \tag{36}$$

$$\omega_j = \frac{1}{2m+1} \quad j = -m, \ldots\ldots, +m$$

being $\omega_{-m} + \ldots + \omega_0 + \ldots + \omega_m$ the weights for the adjusted series mean.

 To soften the available time series, the Henderson moving average, here M_{21}, has been used. Its amplitude is $2m+1 = 21$, and the weight values are,

$$\omega_j = \frac{\nu_j}{3059} \quad j = -10, -9, \ldots\ldots, 10$$

3.3.2   Maximum, mean and median trends

TMY can describe both, daily global solar irradiation and daily sunshine duration (see [20, 21]). At a considered location, the relevant climatic parameters evolution can be represented generating a characteristic year series by means of a one year duration series. This is the TMY. It is necessary to compute the daily typical meteorological year of maximums, means, medians, variance and percentiles of 90% and 75% series of values. In order to improve the knowledge of solar intensities, one TMY for each of those series is obtained using weight means to smooth the irregular data. Finally, the TMY series has to be fitted to a third grade Fourier series. Once all the TMY series are analyzed, the real trend of the global irradiation

behaviour in every location is represented by the median TMY series because means are more susceptible to spurious data.

The proposed model to represent daily time series for radiation is:

$$\frac{T_d - Z_{ad}}{s_d} - M = z_{ad} \tag{37}$$

where $d = 1, \ldots, 365$ and $a = 1, \ldots, A$ being A the number of years with data. M is the average of all the original values Z_{ad}, s_d the series variance, and z_{ad} is the residual ARMA series computed using (34).

For means, we have used the moving average M_{21},

$$\hat{m}_d = \frac{1}{A} \sum_{a=1}^{A} M_{21} Z_{ad} \qquad d = 1, 2, \ldots, 365 \tag{38}$$

In the other hand, the median series is,

$$M'_d = median(Z_{ad}) \qquad a = 1, \ldots, A \qquad d = 1, 2, \ldots, 365 \tag{39}$$

As always, the Henderson moving average was used,

$$M_d = M_{21} M'_d \qquad d = 1, 2, \ldots, 365 \tag{40}$$
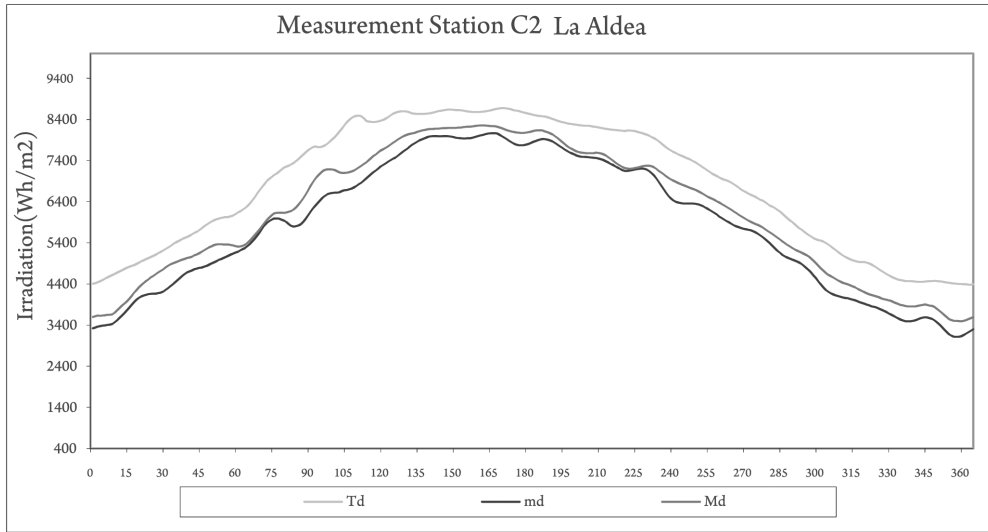
Figure 3. TMY trends for station C2 - *La Aldea* in Gran Canaria Island (Spain)

As an example, the TMY trends for one measurement station can be seen in Figure 3.

4   Irradiation maps

One of the aims of this Chapter is to explain how an irradiation map can be obtained. Thus far, we have reviewed how to define the terrain where we want to know the radiation values,

how to calculate these values for an instant, and how to take into account the cast shadows for every hour. Therefore, we are ready now to apply the concepts explained above and obtain the mentioned maps.

The first step consists in defining the zone to be under consideration. In this Chapter we will use the island of Gran Canaria (Canary Islands - Spain) as our objective, by way of example. The island capital coordinates are $28°06'$ latitude and $-15°25'$ longitude. The UTM coordinates (metres) that define the corners of the considered rectangular domain including the island are $(417025, 3061825)$ and $(466475, 3117475)$, respectively. Using the refinemet/derefinement parameters as explained by Montero et al. [4], a mesh with 5866 nodes and 11683 triangles was built to describe the orography (see Figure 4) and albedo of the island. To define the albedo, the different types of land use in Gran Canaria Island have been studied. The Spanish *Consejo Superior Geográfico* states eleven different types of land for this island. In this simulation, the albedo of the zone varies from 0.05 (Macaronesic laurisilva) to 0.6 (Salt mine) (see Figure 5). The available measurement stations[1] for the island are described in Table 1, and its position can be seen in Figure 4. Starting from the
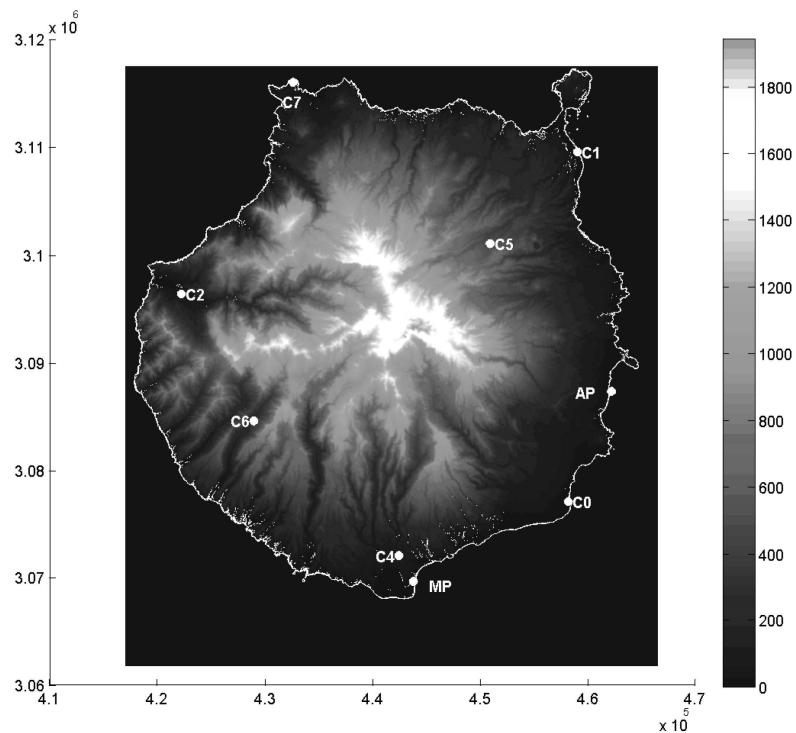
Figure 4. Elevation map of Gran Canaria Island

albedo and topography data, we will construct a mesh of triangles which must be adapted to the geographical characteristics of the terrain by using a refinement/derefinement procedure which takes into account elevation and albedo maps, simultaneously. Height and albedo

---

[1]Courtesy of the *Instituto Tecnológico de Canarias*

Table 1. Geolocation of different measurement stations on Gran Canaria Island.

Station	label	latitude	longitude	height
Pozo Izquierdo	C0	27.8175 N	15.4244 W	47
Las Palmas de G. C.	C1	28.1108 N	15.4169 W	17
La Aldea de San Nicolás	C2	27.9901 N	15.7907 W	197
San Fernando de M.	C4	27.7716 N	15.5841 W	265
Santa Brígida	C5	28.0337 N	15.4991 W	525
Mogán (village)	C6	27.8839 N	15.7216 W	300
Sardina de Gáldar	C7	28.1681 N	15.6865 W	40
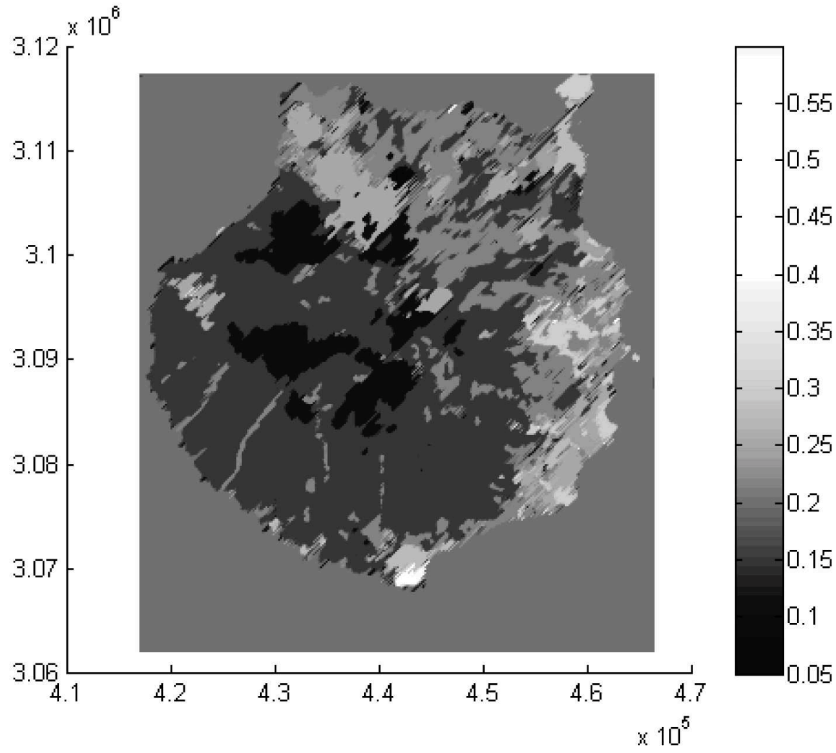
Figure 5. Albedo distribution for Gran Canaria Island

must be known at each point of the mesh and, thus, they have to be interpolated from elevation and albedo mappings, respectively. Of course, great variations in topography or albedo implies more points to define the mesh, this is, we will have triangles from a few kilometres (e.g., on the sea) to a few metres (e.g., on steep slopes) of edge length. To obtain a good accuracy, we chose $\varepsilon_h = 130$ and $\varepsilon_a = 0.08$, so that a mesh with 5866 nodes and 11683 triangles was built to define Gran Canaria Island (see Figure 6). Obviously, this is not the only possible mesh. If we choose diferent values for ε_h and ε_a, we will obtain different meshes. We will get a coarse one with 2164 nodes and 4247 triangles when we
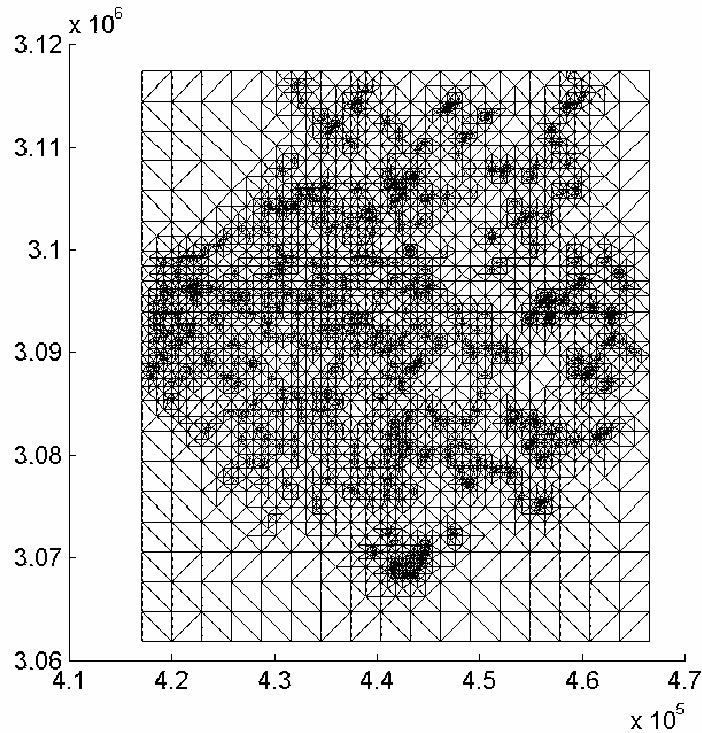
Figure 6. Triangular mesh adapted to topography and albedo

use $\varepsilon_h = 240$ and $\varepsilon_a = 0.10$. Finally a fine one, containing 9276 nodes and 18462 triangles, can be constructed with $\varepsilon_h = 100$ and $\varepsilon_a = 0.07$. Both meshes can be seen in Figure 7. Once the terrain and albedo characteristics have been modelled by means of a mesh, the solar radiation equations seen in section 3 can be applied. The obtained results for each and every time step of a day (e.g. an hour) need to be weighted by the shade analysis done in 2.2. Beam, diffuse and reflected radiations are comptued using the above mentioned equations, and taking into account the calculated shadow distribution on the mesh. Then, for each day, the clear sky global irradiance is computed with the desired time step, as the addition of the three components. Diffuse radiation calculation implies the need of knowing the Linke turbidity factor which can be obtained online from the SoDa Service [31] for each month.

Now that all the irradiance values are calculated for every time step, if we want to know the actual energy as radiation that reachs any point of the mesh, we will have to integrate the irradiance, for example, along a day. For this purpose we have used the Simpson formula to integrate these data numerically in order to obtain the daily radiations. In Figure 8 we can see the flow of actions to obtain the daily irradiation values for real sky conditions. Please note that, as it is said in Figure 8, we will need to use the clear sky index computed through all the measurement stations available over the considered zone and, after that, apply an interpolation of this index for the whole region. This was explained in section 3.2.

Now we are able to draw an irradiation map for a time period. As we can have the irradiation values for any point of the mesh and for a day or a month, it is easy to convert
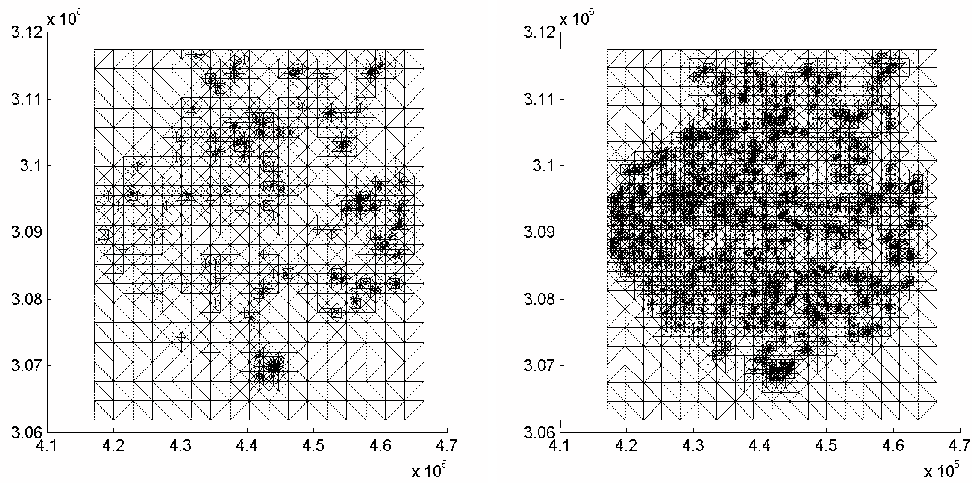
Figure 7. Coarse (left) and fine (right) triangular meshes adapted to topography and albedo
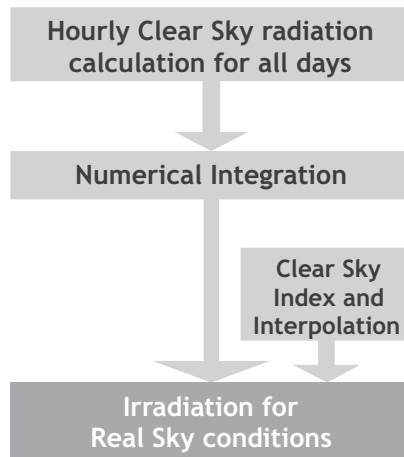
Figure 8. Actions flow to obtain irradiation values

these numerical data into a picture. For example, we can see the irradiation map of Gran Canaria Island for December (TMY), for clear sky conditions. In Figure 9, beam (left) and diffuse (right) radiation maps (J/m^2) are presented for December TMY. In Figure 10 we can see the reflected and global radiation for the same month.

If we take a look at the obtained results, we can see that, under clear sky conditions, beam, diffuse and reflected radiation values are about $82-87\%$, $13-18\%$ and $0-0.5\%$ of the mean global radiation respectively.

Figure 11 shows the global irradiation map for the island under real sky conditions for December considering a typical meteorological year. The monthly daily average real sky global radiation, for the whole studied region of the example (Gran Canaria Island), varies from 10.6, MJ/m^2 per day in December, to 25.6, MJ/m^2 per day in June (see Figure 12). In
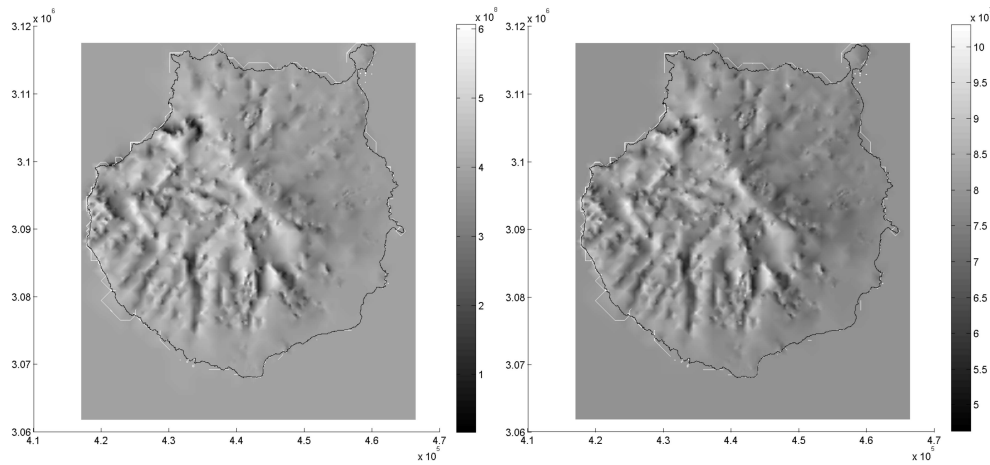
Figure 9. Beam (left) and Diffuse (right) radiation maps (J/m^2) for December TMY
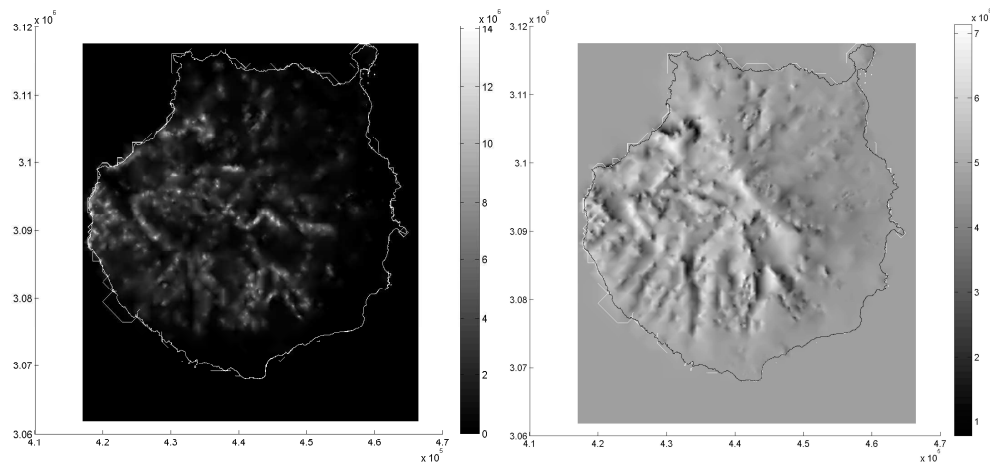
Figure 10. Reflected (left) and Global (right) radiation maps (J/m^2) for December TMY

this Figure we can see the annual evolution of the computed monthly average per day for both, clear sky and real sky global radiation.

Taking a look at the differences between both curves we obtain Figure 13, where the percentage decrease from the computed radiation is presented. In this Figure we observe the radiation behaviour for our example, where the most clear days over the whole island are those from Spring, especially during the months of May and June. We can see the typical behaviour of the cloudiness produced by the Trade Winds over the island during Summer. The months of July and August show a separation from the trend that would be expected when we are talking about this season. That decrease in the radiation level over the whole island is caused by the above mentioned cloudiness which affects in Summer to the northern part of the island.

Below (Figure 14) we can see the global real sky irradiation maps for the months of
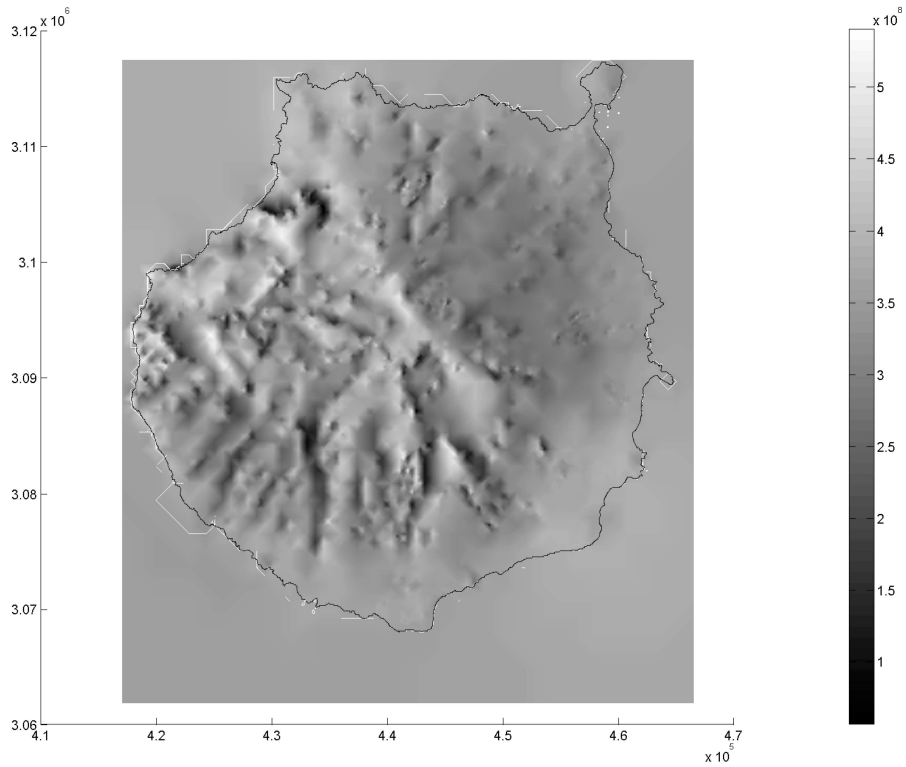
Figure 11. Global Real Sky radiation map (J/m^2) for December TMY
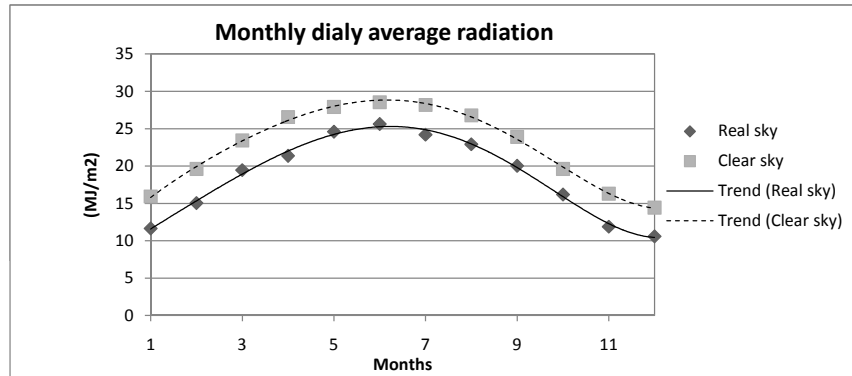
Figure 12. Monthly average radiation per day

June and September TMY and a southeast three-dimensional view of the same radiation map for the TMY month of March (Figure 15).
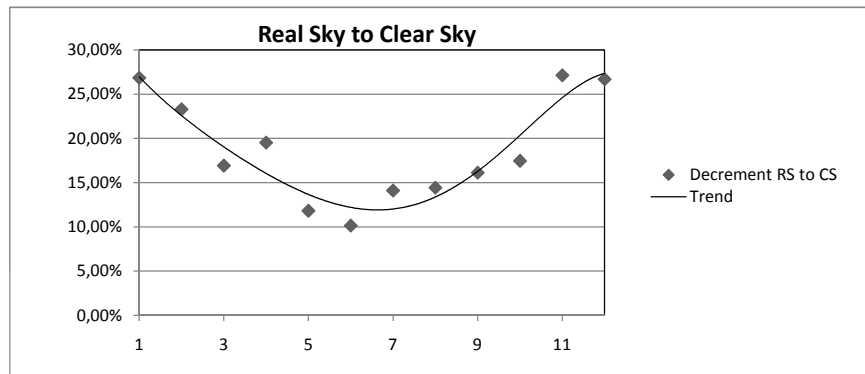
Figure 13. Percentage decrease in computed radiation
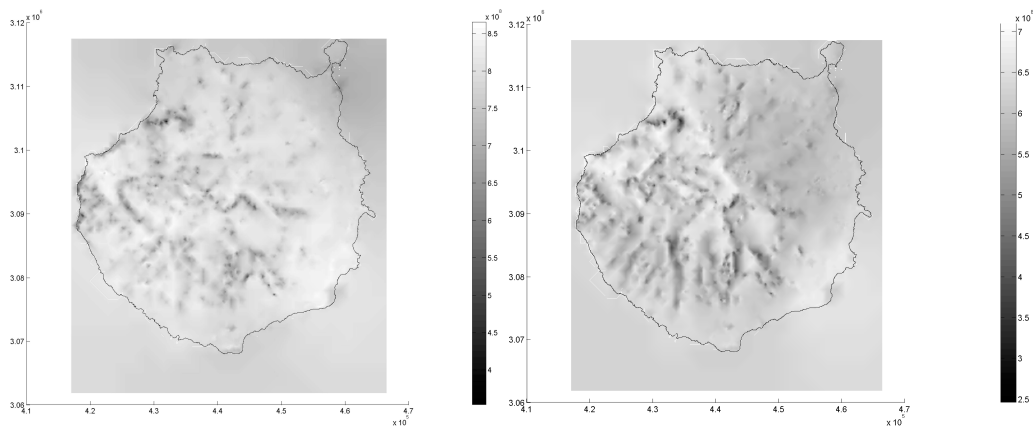
Figure 14. Global Real Sky radiation map (J/m^2) for June (left) and September (right)

5   Irradiance graphs

The previous section showed the distribution maps for irradiation as described by ISO 9488, this is, the radiation energy density that comes into contact with the terrain. Irradiation maps are very useful to find the best places in a zone where to install a solar power station from the perspective of the energy maximization, or, for example, simply for climate analysis or for farming production objectives.

However, solar radiation incidence on the terrain is not constant along the day. As e-verybody knows, radiation increases from zero at dawn, up to a maximum at noon and then decreases until the sunset, when it becomes zero again. Of course, what we have computed in previous sections was the integration of these radiation curves along a day. This irradia-tion per time unit is the *irradiance*, usually given in W/m^2. The analysis of irradiance values and graphs is of utmost importance when it comes to studying the electric power generation through solar radiation conversion. An irradiance graph for a TMY particular day, allows us to know the electric power production per hour (or per another time step) what can be of big
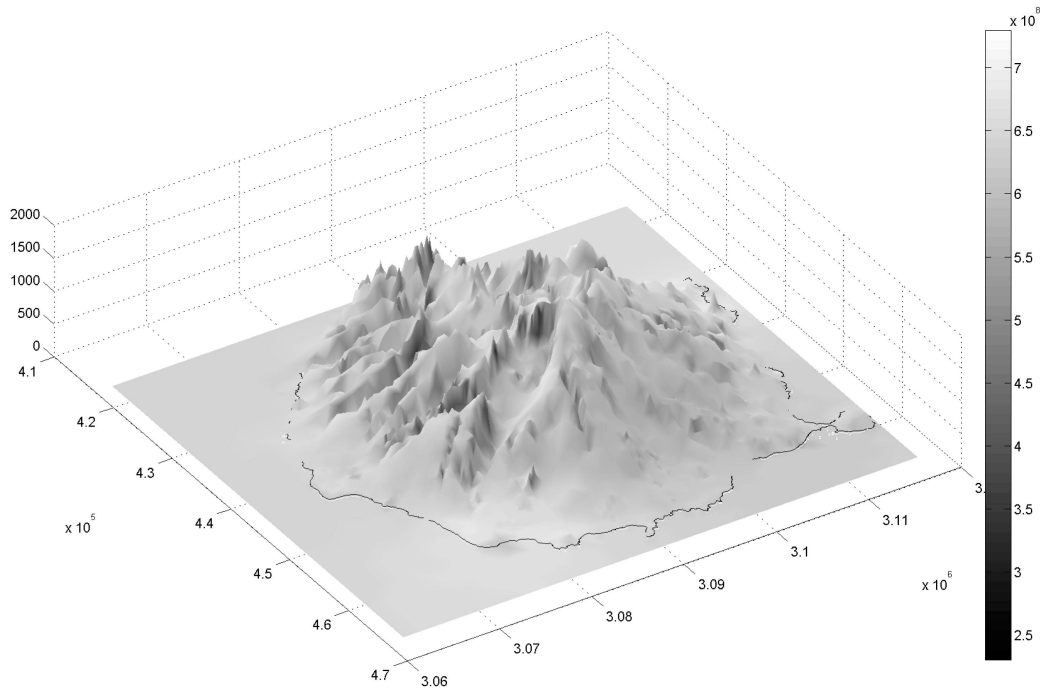
Figure 15. 3D global Real Sky radiation map (J/m^2) for March

help when trying to make an optimal electric power dispatch in case of having a high solar energy penetration in the electric power system. This fact is increasingly more likely due to the growth of solar power installed, whether it be photovoltaic or solar thermal power.

At this point, the process to obtain the irradiance is very simple. Actually, we already do have irradiance values, since we integrated them as showed in Figure 8. In Figure 16, the actions flow for the extraction of the irradiance values is showed. The calculation of the subsequent conversion to electric power is easy introducing the models of photovoltaic and/or solar thermal power conversion.

With regard to the real sky irradiance, it will be calculated (Figure 16) using the clear sky index values obtained by means of equation 32 and considering a linear distribution along the day. This is done to avoid an extremely high computational cost. If more accuracy is needed, k_c can be calculated for every time step as long as there are available data. In Figure 17, the calculated irradiance in *Maspalomas*[2] for clear and real sky are showed for January, 15th (left) and July, 15th (right). All values are calculated assuming a horizontal surface. The abscissa are the *Coordinated Universal Time* (UTC) for Gran Canaria Island, which is around one hour forward respect to the local solar time. As said above, irradiance graphs allow us to know the evolution of the electric power generated through a photovoltaic or solar thermal conversion. In these cases, the surface that receives the radiation is generally not horizontal. As the objective is to maximize the energy production, photovoltaic panels or solar thermal collectors will have a certain inclination respect the terrain in order

---

[2]South of Gran Canaria Island, next to C4 Station -see Fig. 4-
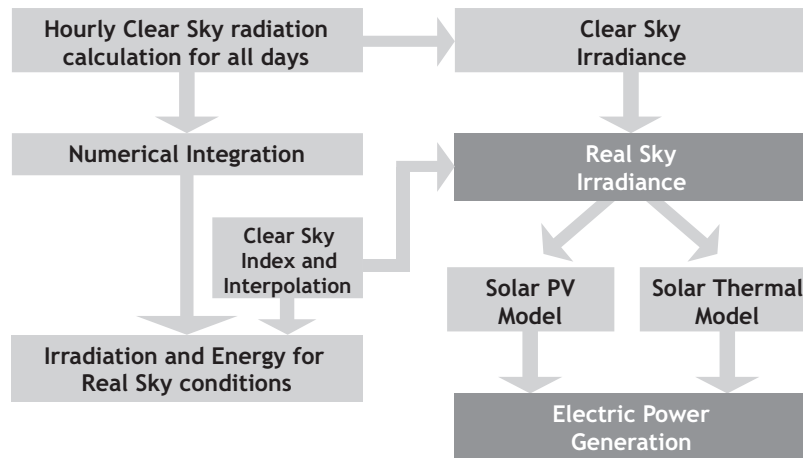
Figure 16. Actions flow to obtain values for irradiance and electric power generation
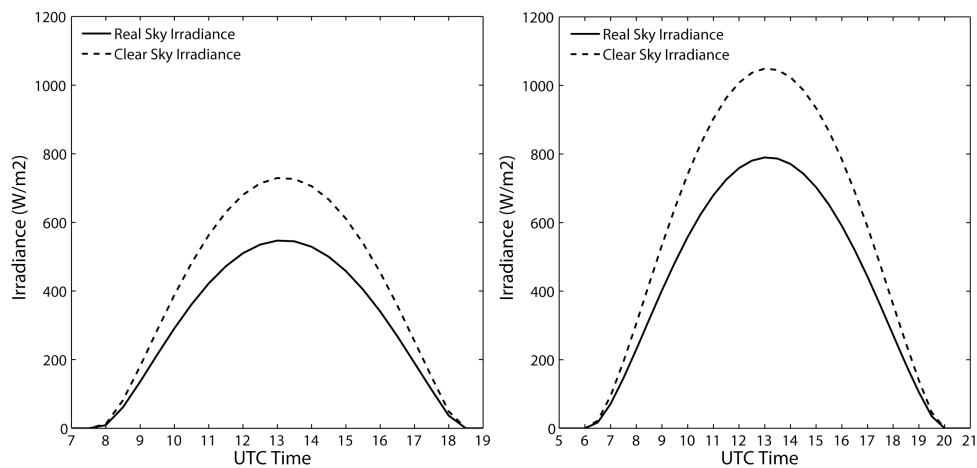
Figure 17. Daily irradiance (W/m^2) for Maspalomas. January (left). July (right)

to get the maximum solar radiation. The optimal inclination depends on the latitude of the zone under study and, of course, on the month, day and time to be considered. Therefore, this angle is desirable to be changed along the year though it is very common to find solar facilities, especially in photovoltaics, with fixed inclination collectors to reduce costs.

Due to the great importance of the solar energy conversion into electric power, it is suitable to use the model with surfaces inclined respect the horizontal. The way to achieve this goal is considering a photovoltaic panel or a solar thermal collector, inserted in the terrain mesh by means of two or more triangles with the desired inclination and then, calculate the irradiance over it. That is how figures 18 and 19 have been done. In them, we can see the daily irradiance for a south oriented collector in Maspalomas, July the 15th with different inclinations and with a time step of 30 minutes. Maximum irradiance (see Table 2 is obtained with a collector inclination of 10° at 13 UTC (12 solar local time). Please note

that maximum irradiance does not implies a maximum daily irradiation because the panel orientation (south in this case) affects the incidence of the sun rays at the first and last hours of the day what causes small differences between the irradiance integrals.
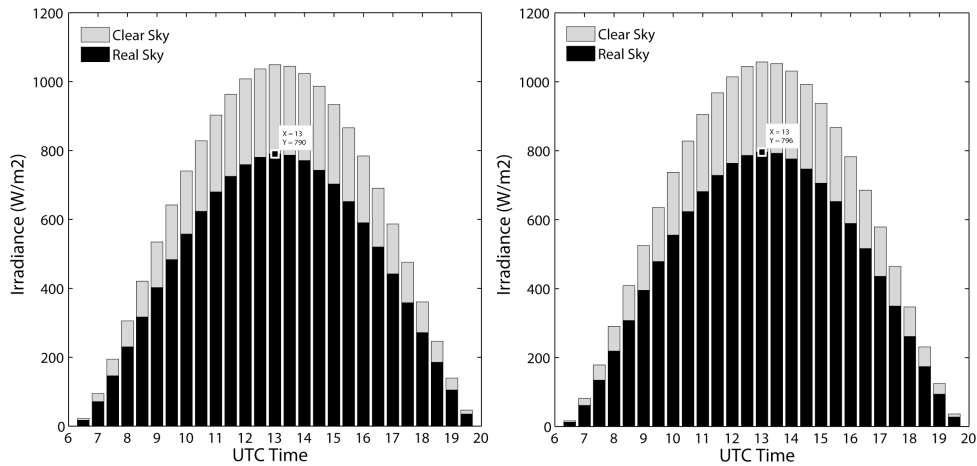
Figure 18. Daily irradiance for Maspalomas, July 15th. Panel inclination: 0^o(L), 5^o(R)
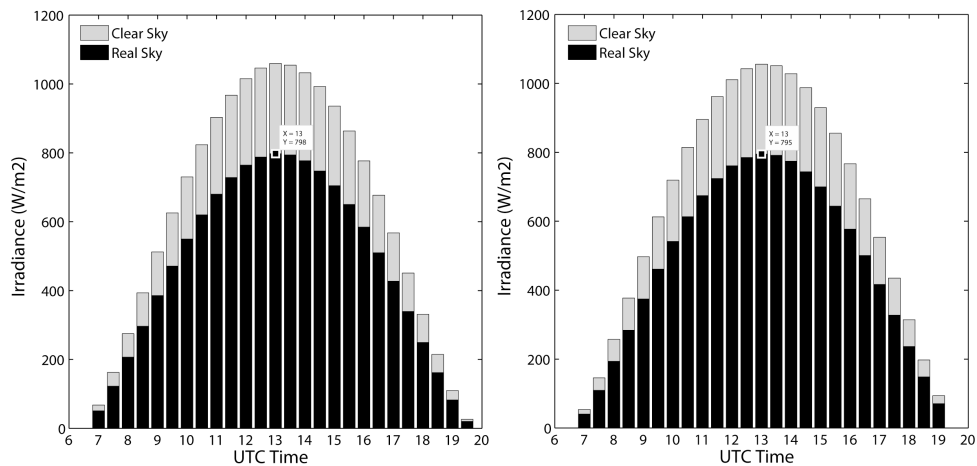
Figure 19. Irradiance for Maspalomas, July 15th. Panel inclination: 10^o(L), 15^o(R)

Table 2. Maximum irradiance. Maspalomas, July the 15th, 13 UTC

Collector inclination	0°	5°	10°	15°
Irradiance (W/m^2)	790	796	798	795

This numerical model allows to evaluate the irradiance for different orientations and

inclinations. As an example, the daily irradiance on a collector inclined 60° and oriented east or west, is presented in Figure 20. The left figure shows the east oriented collector, and the right one the west oriented. The studied point is in Las Palmas de Gran Canaria (north of the island) and the date is January, 15th. It is obvious that both curves are now asymmetrical. The east oriented panel receives higher irradiance values during the first hours in the morning, with a maximum at 10:30 UTC (time steps of $1/2$ hour) of 566.3 W/m^2. On the contrary, the west oriented one receives more irradiance during the second half of the day, with a maximum value of 567.8 W/m^2 at 16 UTC.
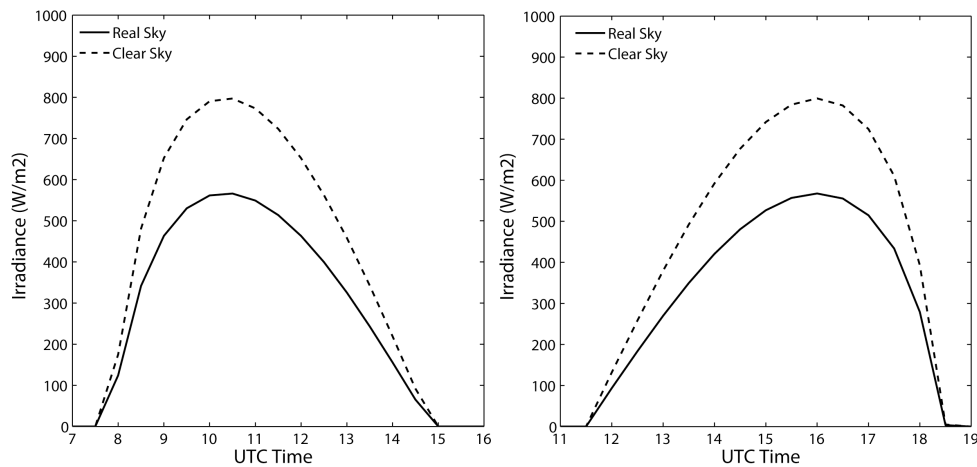
Figure 20. Irradiance for Las Palmas de Gran Canaria, January 15th. Panel inclination: 60°. Orientation: East (L), West (R)

In case of photovoltaic or solar thermal power exploitation, especially with high solar energy penetration in the electric power system, an optimal power dispatch is needed. The problem is that we really do not know the exact electric power that can be produced tomorrow or the day after tomorrow. Moreover, to adjust the electric generation to the particular Load Curve of a system, we need to know the solar power along the day, the actual daily solar power hour by hour, but that is simply impossible. Most that can be done is a prediction of the power generated hour by hour. This prediction would have to be based on a weather forecast that estimates some local weather variables which allow us to know if it is probable to have a cloudy or sunny day at any hour. Therefore, what we need is to adjust the clear sky index k_c hour by hour, to draw an irradiance graph that takes into account the presence of clouds in the hours that they are expected, this is, to calculate different k_c depending on the hour. What is new in this approach respect to what was done above? The answer is easy: Our first approach was applying the clear sky index in a linear way along the day. Now, that index can have different values for each hour. The rest of the procedure would be the same as explained above.

6   Conclusions

A numerical model for estimating the solar radiation on a surface is presented. Needed requirements are the location, topography, albedo and observational data. Solar radiation on a surface is estimated taking into account the shadow distribution in each time step. For this purpose, the adaptivity of the triangulation related to the topography and albedo is essential. Adaptive meshes lead to a minimum computational cost, since the number of triangles to be used is optimum [4].

A *Typical Meteorological Year* (TMY) [21] is needed to convert the clear sky into real sky radiation values. To calculate these, we propose an interpolation method which is suitable when a considerable number of stations is available and they are well distributed in the zone under study. Another procedures, such as spline functions for interpolating the clear sky index on the surface (see e.g. [32]) can be applied. Solar power generation, photovoltaic or solar thermal, can be estimated from real sky values, taking into account the models of the different power station parts. Moreover, rectangular collectors can be included in the model as composed by two triangles in the same plane, with a given inclination and orientation.

The model allows estimating the irradiance for any day (TMY) with the desired time step. This could be a big help in forestry, agronomy or electrical engineering. It can be an interesting tool regarding to the optimal power dispatch in case of having solar power generation. For this purpose we need to add meteorological information (for example from MM5, WRF, HIRLAM) to obtain a predictive solar radiation model.

7   Acknowledgments

References

[1] M. Šúri, J. Hofierka, "A New GIS-based Solar Radiation Model and its application to photovoltaic assessments", Transactions in GIS 8 (2), 175–170. 2004.

[2] M. Šúri, J. Hofierka, "The solar radiation model for Open source GIS: implementation and applications". In: Benciolini, B., Ciolli, M., Zatelli, P. (Eds.), Proceedings of the Open source GIS-GRASS users conference, Trento, Italy, 1–19, 2002.

[3] E. Cogliani, P. Ricchiazzi, "Generation of operational maps of global solar irradiation on horizontal plan and of direct normal irradiation from Meteosat imagery by using SOLARMET", Solar Energy 82 (6), 556–562, 2008.

[4] G. Montero, J.M. Escobar, E. Rodríguez, R. Montenegro, "Solar radiation and shadow modelling with adaptive triangular meshes", Solar Energy 83 (7), 998–1012, 2009.

[5] F. Díaz, G. Montero, J.M. Escobar, E. Rodríguez, R. Montenegro, "A Solar Radiation Model for Photovoltaic and Solar Thermal Power Exploitation", Proceedings of the Seventh International Conference on Engineering Computational Technology, Valencia, Spain, paper 172, 2010.

[6] A. Niewienda, F.D. Heidt, "SOMBRERO: a PC-tool to calculate shadows on arbitrarily oriented sufaces", Solar Energy 58 (4-6), 253–263, 1996.

[7] K. Zakšek, T. Podobnikar, K. Oštir, "Solar radiation modelling", Computers & Geosciences 31 (2), 233–170, 2005.

[8] J. Dozier, J. Bruno, P. Downey, "A faster solution to the horizon problem", Computers & Geosciences 7, 145–151, 1981.

[9] A.J. Stewart, "Fast horizon computation at all points of a terrain with visibility and shading applications", IEEE Transactions on Visualization and Computer Graphics 4 (1), 82–93, 1998.

[10] G. Winter, G. Montero, L. Ferragut, R. Montenegro, "Adaptive strategies using standard and mixed finite element for wind field adjustment", Solar Energy 54 (1), 46–56, 1995.

[11] L. Ferragut, R. Montenegro, A. Plaza, "Efficient refinement/derefinement algorithm of nested meshes to solve evolution problems", Comm Num Meth Engrg 10, 403–412, 1994.

[12] G. Montero, E. Rodríguez, R. Montenegro, J.M. Escobar, J.M. González-Yuste, "Genetic algorithms for an improved parameter estimation with local refinement of tetrahedral meshes in a wind model", Advances in Engineering Software 36, 3–10, 2005.

[13] G. Montero, R. Montenegro, J.M. Escobar, E. Rodríguez, J.M. González-Yuste, "Velocity field modelling for pollutant plume using 3-D adaptive finite element method", Lecture Notes in Computer Science 3037, 642–645, 2004.

[14] M.C. Rivara, "A Grid Generator Based on 4-Triangles Conforming. Mesh-Refinement Algorithms", Int J Num Meth Engrg 24, 1343–1354, 1987.

[15] A. Plaza, R. Montenegro, L. Ferragut, "An improved derefinement algorithm of nested meshes", Advances in Engineering Software 27 (1-2), 51–57, 1996.

[16] J.W. Gruter (ed), "Radiation Nomenclature". Brussels, CEC, Second Solar Energy Programme, Project F, Solar Radiation Data, 1984.

[17] M. Blanco-Muriel, D.C. Alarcón-Padilla, T. López-Moratalla, M. Lara-Coira, "Computing the solar vector", Solar Energy 70 (5), 431–441, 2001.

[18] J. Krcho, "Morfometrická analýza a digitálne modely georeliéfu", Veda, Bratislava, 1990.

[19] M. Jenčo, "Distribúcia priameho slnecného žiarenia na georeliéfe a jej modelovanie pomocou komplexnho digitálneho modelu georeliéfu", Geografický casopis 44 (4), 342–354, 1992.

[20] L. Mazorra, F. Díaz, P. Navarro, "Estimation of global solar radiation by means of sunshine duration", Proceedings of ISES Solar World Congress: Solar energy and human settlement, Beijing, China, Vols. I-V, pp. 2627–2631, 2007.

[21] L. Mazorra, F. Díaz, G. Montero, R. Montenegro, "Typical meteorological year (TMY) evaluation for power generation in Gran Canaria Island, Spain", Proceedings of 25th European Photovoltaic Solar Energy Conference and Exhibition and 5th World Conference on Photovoltaic Energy Conversion, Valencia, Spain, 4726–4728, 2010.

[22] J.K. Page (ed), "Prediction of Solar Radiation on Inclined Surfaces", D. Reidel Publishing Co., Dordrecht, 1986.

[23] F. Kasten, "The Linke turbidity factor based on improved values of the integral Rayleigh optical thickness", Solar Energy 56 (3), 239–244, 1996

[24] F. Kasten, A.T. Young, "Revised optical air mass tables and approximation formula", Applied Optics 28, 4735–4738, 1989.

[25] K. Scharmer, J. Greif, "The European Solar Radiation Atlas.Vol. 2 : Database and exploitation software", Les Presses de l'École des Mines, Paris, 2000.

[26] T. Muneer, "Solar Radiation model for Europe", Building Services Engineering Research and Technology 11, 153–163, 1990.

[27] T. Muneer, "Solar Radiation and Daylight Models for Energy Efficient Design of Buildings", Architectural Press, Oxford, 1997.

[28] G. Montero, R. Montenegro, J.M. Escobar, "A 3-D Diagnostic Model for Wind Field Adjustment", J Wind Engrg Ind Aer 74-76, 249–7261, 1998.

[29] A. Argiriou, S. Lykoudis, S. Kontoyiannidis, C. A. Balaras, D. Asimakopoulos, M. Petrakis, P. Kassomenos, "Comparison of methodologies for tmy generation using 20 years data for Athens, Greece", Solar Energy 66 (1), 33–45, 1999.

[30] R. Aguiar, M. Collares-Pereira, "TAG: A time-dependent, autoregressive, Gaussian model for generating synthetic hourly radiation", Solar Energy 49 (3), 167–174, 1992.

[31] SoDa Service (Solar Data), "Services for Professionals in Solar Energy and Radiation". Available at $http : //www.soda − is.com/eng/services/service\_invoke/gui.php$.

[32] Y. Xia, M. Winterhalter, P. Fabian, "Interpolation of Daily Global Solar Radiation with Thin Plate Smoothing Splines", Theor Appl Climatol 66, 109–115, 2000.